An Experimental Study of Unsteady Behaviour of Cavity Flow Over a 2-D Wall-Mounted Fence

[1]Luka Barbaca*; [1]Bryce W. Pearce; [1]Paul A. Brandner; [2]Harish Ganesh; [2,3]Steven L. Ceccio

[1]*Australian Maritime College, University of Tasmania, Launceston, Tasmania, Australia*

[2]*Department of Mechanical Engineering, University of Michigan, Ann Arbor, MI, USA*

[3]*Department of Naval Architecture and Marine Engineering, University of Michigan, Ann Arbor, MI, USA*

Abstract

The unsteady behaviour of ventilated and natural cavity flows over a 2-D wall-mounted fence is investigated for fixed length cavities with varying free-stream velocity using still imaging, X-ray densitometry and dynamic surface pressure measurement in two experimental facilities. Cavities in both ventilated and natural flows were found to have a re-entrant jet closure, but not to exhibit large-scale oscillations, rather irregular small-scale shedding at the cavity closure. Small-scale cavity break-up was associated with a high-frequency broad-band peak in the wall pressure spectra, found to be governed by the overlying turbulent boundary layer characteristics, similar to observations from single-phase flow over a forward-facing step. A low-frequency peak reflecting the oscillations in size of the re-entrant jet region, analogous to 'flapping' motion in single-phase flow, was found to be modulated by gravity effects (i.e. a Froude number dependence).

Keywords: cavitation; ventilation; wall-mounted fence

Introduction

Flow over a geometric discontinuity immersed in a turbulent boundary layer will result with flow separation. Cavitation may occur in a separated flow region as the local pressure approaches vapour pressure. As the cavitation number is reduced the gaseous bubble/cavity grows and eventually surpasses the original length of the separated flow region [6]. Depending on the location of the cavity closure, i.e. if the closure is on the wall of the cavitating body or rather downstream, cavities are classified as either 'partial' or 'super-cavities'. Cavities of similar appearance and behaviour, termed 'ventilated' can be formed artificially if sufficient gas (typically air) is injected into the separated flow region [11]. It is the condition of the cavity closure on the wall that is responsible for the emergence of significant unsteadiness in flows featuring partial cavitation. The closure region of an unsteady partial cavity is found to generally exhibit a re-entrant jet behaviour.

In a seminal study Callenaere et al. [5] were able to map various cavitation regimes, among which they differentiated two regimes with the established re-entrant jet flow based on the re-entrant jet to cavity thickness ratio. In the case of the re-entrant jet being much thinner than the cavity, the classical cloud cavitation instability characterized by the re-entrant jet propagation up to the cavity leading edge and periodic shedding of large-scale bubbly structures is observed. In the second regime, labelled as 'thin non-auto-oscillating cavities with periodic re-entrant jet', the re-entrant jet thickness is relatively large compared to the cavity thickness, promoting interaction between the jet/cavity and cavity/water interfaces. The small-scale instability resulting from this interaction induces cavity break-up at many random points, leading to irregular shedding of a large number of small-scale structures and a globally quasi-steady cavity appearance. Due to the less severe effect on the flow this second regime type has received little attention in comparison with cloud cavitation.

Until the recent numerical and experimental studies reported by the authors [12, 2, 1, 3], cavity flow over a wall-mounted fence has not been reported on in the open literature. To date the mean characteristics and global behaviour of the cavity flow over a fence immersed in an oncoming wall boundary layer of variable thickness for a range of free-stream conditions has been reported on. The next step towards a better understanding of this canonical flow with a nominally zero stream-wise pressure gradient is to analyse unsteady behaviour.

Within the present study the unsteady behaviour of ventilated and natural cavity flow over a 2-D wall-mounted fence is experimentally investigated in two testing facilities. Large-scale experiments are performed in the University of Tasmania water tunnel with a 600 $\times$ 600 mm square test section, whilst smaller-scale experiments are performed in

*Corresponding Author, Luka Barbaca: Luka.Barbaca@utas.edu.au

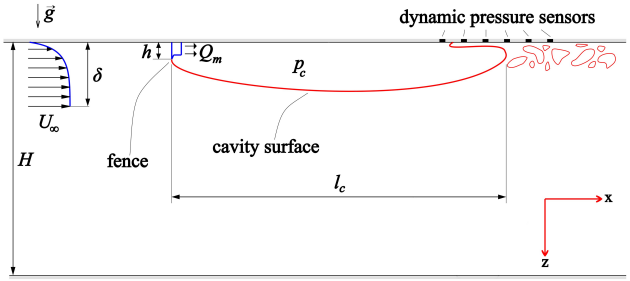

Figure 1: Sketch of a wall mounted fence immersed in the oncoming wall boundary layer with a cavity detaching from the sharp fence tip. The location along the test-section ceiling centre-line of an array of six dynamic pressure sensors in the cavity closure region is indicated.

the University of Michigan 9-inch water tunnel with the test section size reduced to 76.2 $\times$ 76.2 mm. These experimental setups are developed to utilize the complimentary capabilities from each facility, with X-ray densitometry measurements from the small-scale experiment and long-period pressure measurements from an array of six dynamic pressure sensors from the large-scale tests. The scope of work is to examine the influence of free-stream Reynolds and Froude numbers on the cavity closure dynamics and the mechanisms of gas entrainment into the main flow for a fixed cavity length to fence height ratio.

1 Experimental Overview

A schematic of cavity flow over a wall-mounted fence representative of the tests in both facilities is shown in figure 1. A fence of height h is immersed in the upstream wall boundary layer of thickness δ. In the case of a ventilated cavity, air is supplied to the wake region of the resulting bluff body flow with a mass flow rate Q_m. Alternatively, for $Q_m = 0$, a natural cavity may be formed due to phase change when the pressure in the wake of the fence, $p = p_c$, reduces to vapour pressure, p_v. Irrespective of the type of formation (i.e. natural or ventilated), the cavity detaches from the sharp fence tip and exhibits a re-entrant jet closure region.

The flow dependence on the free-stream velocity has been quantified using fence height based Reynolds ($Re_h = U_\infty h/\nu$, where U_∞ is the reference free-stream velocity and ν is the kinematic viscosity of the water) and Froude numbers ($Fr_h = U_\infty/\sqrt{gh}$, where g is the gravitational acceleration). For the characterization of unsteady behaviour of the flow a fence height based Strouhal number is used, $St_h = fh/U_\infty$, where f is the frequency of the unsteady phenomenon of interest.

The large-scale experiments were performed in the University of Tasmania variable pressure water tunnel. Detailed description of the facility and the instrumentation used can be found in Barbaca et al. [3]. The fence model incorporating an internal air supply channel is machined from a stainless steel bar, with a manifold for air distribution attached to the downstream face. The fence is 599 mm wide $\times$ 10 mm high, with a sharp tip machined on the front face to ensure a stable cavity detachment. Air is supplied through the fore-body of the fence to the manifold, from which it is distributed into the wake of the fence through 40 $\times$ ϕ2 mm equi-spaced stream-wise outlets. The fence is located 230 mm from the test section entrance, with the oncoming wall boundary layer thickness at this stream-wise position being 15 mm [4], giving a boundary layer thickness to fence height ratio of $\delta/h = 1.5$.

An array of six flush-mounted 8.1 mm diameter FUTEK PFT510 dynamic pressure sensors installed within the test-section ceiling window was used for the measurements of unsteady pressure within the cavity closure region. The most upstream sensor was located 730 mm downstream of the fence tip, with each subsequent sensor positioned 60 mm further downstream along the test-section horizontal centre-line. The sensor range is 15 bar absolute, with a rated output of $1-2$ mV/V (estimated output uncertainty of 0.8%) and natural frequency of 6 kHz. A 5V excitation and signal amplification is provided through an Entran MSC6 signal conditioning box, with data acquired simultaneously using a National Instruments PXIe-4497 card. High-resolution front-lit still images were captured using a Nikon D810E camera with a Nikon Nikkor f/2.8D 24mm lens.

Natural and ventilated cavities of nominally fixed length, $l_c/h \approx 90$, were investigated for a range of free-stream speeds. Tests were conducted over the full operational range, $2 \leq U_\infty \leq 12$ m/s, resulting in Reynolds and Froude numbers varying between $2 \times 10^4 \leq Re_h \leq 1.2 \times 10^5$ and $6.4 \leq Fr \leq 38.3$, respectively. All tests were conducted with a dissolved O_2 content between 2 and 6 ppm.

*Corresponding Author, Luka Barbaca: Luka.Barbaca@utas.edu.au

The small-scale experiments were performed at the University of Michigan 9-Inch Water Tunnel. Detailed description of the facility and the instrumentation can be found in Ganesh et al. [7]. To achieve flow similarity between the two facilities it was decided to have the same δ/h. The fence model spanning the test section width is machined from a 6 mm brass bar and is mounted inside a recess in the acrylic ceiling window. The fence is 75.2 mm wide, with the in-flow height of $h = 1.33$ mm. A sharp tip is machined on the fence front tip to ensure a stable cavity detachment. A gap between the fence body and the recess walls serves as a plenum for air injection which is distributed into the fence wake through a full-span slanted slot between the angled downstream face of the fence and the ceiling. The fence tip is located 115.6 mm downstream of the entrance to reduced test section. The oncoming wall boundary layer thickness at this position is ≈ 2 mm, resulting in $\delta/h \approx 1.5$.
A cinematographic X-ray densitometry system was used to measure the span-wise averaged spatial distribution of the void fraction for the ventilated and natural cavity flows over the fence. A complete description of the X-ray setup and data reduction process is provided by Mäkiharju et al. [10]. The X-ray images were acquired at a sample rate of 1 kHz for ≈ 0.8 s. Ventilated and natural cavities of nominally fixed length, $l_c/h \approx 60$, were investigated for a constant free-stream speed, $U_\infty = 10$ m/s ($Re_h = 1.33 \times 10^4$, $Fr_h = 87.6$). All tests were conducted with a dissolved O_2 content between 2 and 6 ppm.

2 Results

A typical topology of a fully developed ventilated cavity observed in the large-scale test is shown in figure 2 for $Re_h = 1 \times 10^5$. The cavity has a stable detachment from the fence tip and two distinct regions are evident along the cavity length. The region closer to the fence is air/vapour filled with a relatively sharp cavity/water interface and a transparent appearance. The rear or closure of the cavity is dominated by re-entrant jet flow and is observed as an opaque region. From the observation that the re-entrant jet does not propagate all the way upstream to the fence, but is contained to the closure region only, the flow can be classified within the 'thin cavities' regime as distinguished by Callenaere et al. [5]. The opaque cavity surface appearance is a result of interaction between a relatively thick re-entrant flow region and the cavity/water interface, inducing irregular/chaotic cavity surface break-up. The surface break-up triggers the shedding of small-scale bubbly structures into the cavity wake with consequent entrainment into the main flow. This small-scale pinch-off at the cavity closure results in a relatively small variation in the cavity length and the cavity can be considered as non-auto-oscillating.
The main difference between the ventilated and natural cavity flows is observed in the wake region. The wake of a ventilated cavity consists of a dense mixture of shed structures of variable scale. In the case of a natural cavity the vaporous structures condense within a short distance from the closure and only a population of micro-bubbles containing incondensable gas remains in the far wake.
In figure 3 instantaneous void fraction distribution extracted from X-ray imaging, along with the root-mean-square deviation (RMSD) of the X-ray sequence, is shown for the ventilated (a) and natural (b) cavity flows from the small-scale test for $l_c/h \approx 60$ and $Re_h = 1.33 \times 10^4$. Note that the scale in X-ray images is exaggerated (times two) in the vertical direction. From the instantaneous X-ray frames a difference in the mean void fraction distribution can be observed between the ventilated and natural cases. While the upstream part of the cavity has a similar maximum void fraction value in both cases, a more significant difference can be seen in the closure. Firstly, the mean α (void fraction) value is noticeably lower in the naturally cavitating flow across the whole re-entrant jet affected region and secondly, the re-entrant jet itself has a much higher liquid content when compared with a seemingly more bubbly jet present for the

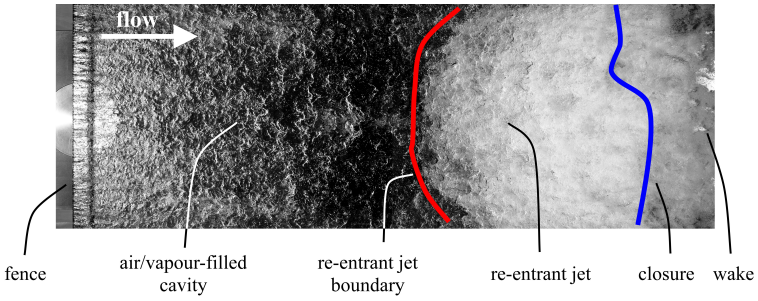

Figure 2: Typical topology of a cavity observed in the large-scale experiments for $Re_h = 1 \times 10^5$. Cavity has an air/vapour filled region present closer to the fence and a re-entrant jet type closure, and can be classified within 'thin cavity' regime as specified by Callenaere et al. [5].

*Corresponding Author, Luka Barbaca: Luka.Barbaca@utas.edu.au

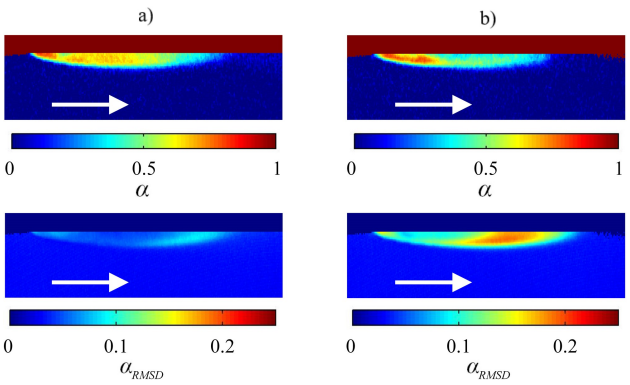

Figure 3: Topologies of ventilated (a) and natural (b) cavity flow from the small-scale experiment for $Re_h = 1.33 \times 10^4$ shown as instantaneous frames extracted from X-ray imaging. Additionally, the root-mean-square deviation (RMSD) of the void fraction (α) from the X-ray sequences is presented for both cases. Note that the scale in the X-ray images is shown exaggerated (times two) in the vertical direction.

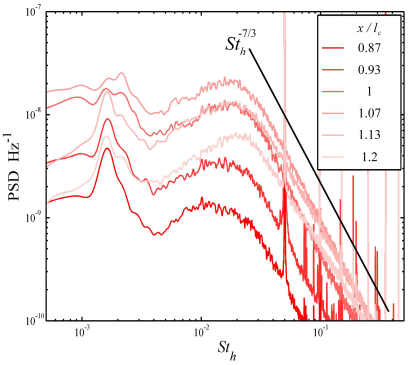

Figure 4: Wall pressure power spectra from six dynamic pressure sensors located on the test-section ceiling centre-line for ventilated flow at $Re_h = 1 \times 10^5$. A black line indicates the power spectra decay following a power law behaviour proportional to $St_h^{-7/3}$.

ventilated flow. From the plots of void fraction RMSD it is observable that the void fraction distribution undergoes much more pronounced oscillations (approximately a 100 % increase in RMSD value) for natural cavitation.

The power spectral densities (PSDs) of long sampled pressure signals from an array of six pressure sensors located in the cavity closure region were analysed using the Welch method. The pressure sensors are positioned with the nominal position of cavity closure approximately aligned with the third most upstream sensor. The time-series were recorded for 1000 s at 1 kHz. In figure 4 ventilated flow pressure spectra from each sensor is given for a constant $Re_h = 1 \times 10^5$. Spectral content observed for each sensor is characterized by two broad-band peaks and a high-frequency roll-off that follows a power law behaviour ($\propto St_h^{-7/3}$). Interestingly, this behaviour in two-phase flow is similar to that observed in the single-phase flow over a forward-facing step [8]. Although, the similarity between the single-phase and cavitating flow is remarkable, a significant difference exists. For two-phase flow peaks in pressure fluctuations are observed at $St_h \approx 0.002$ and $St_h \approx 0.02$, whereas in single-phase flow these peaks occur an order of magnitude higher. The low-frequency peak can be associated with the oscillations of the re-entrant jet length (analogous to 'flapping' motion in single-phase flow), while the high-frequency peak can be related to the cavity break-up induced by the large-scale structures contained within the overlaying turbulent boundary layer. The observed power law like high-frequency power spectra decay characterizes the spectral content of pressure fluctuations within a turbulent boundary layer in a single-phase flow, which further supports the premise that cavity closure break-up is dominated by the characteristics of the overlaying boundary layer.

In figure 5 wall pressure spectra from the sensor nominally aligned with the cavity closure is given for ventilated cavity case for the full range of Re_h investigated. From figure 5a it can be seen that if the PSD is plotted against the Strouhal number defined using a constant length scale (i.e. fence height), the high frequency peak will collapse to a constant $St_h \approx 0.02$ value, leading to a conclusion that the frequency of turbulent shedding is proportional to free-

*Corresponding Author, Luka Barbaca: Luka.Barbaca@utas.edu.au

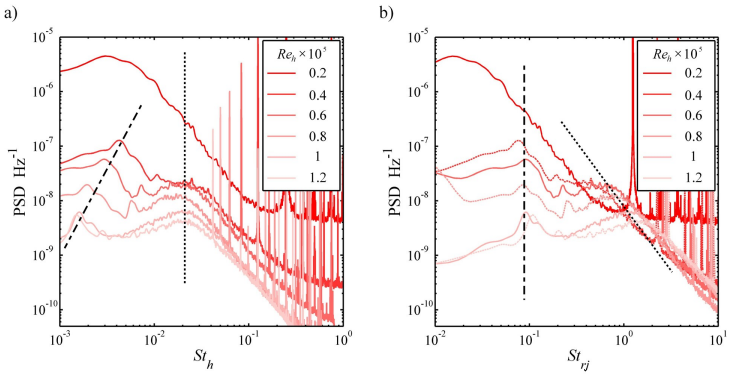

Figure 5: Wall pressure power spectra from the dynamic pressure sensor nominally aligned with the cavity closure. Data is presented for ventilated flow with the frequency non-dimensionalised as St_h (a) and St_{rj} (b). The dash-dot lines are added to the plots to indicate the low-frequency peaks, while the dotted lines denote the high-frequency peaks.

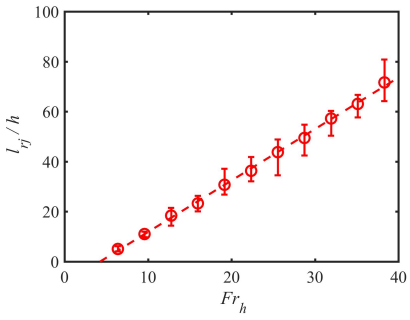

Figure 6: Dependence of non-dimensionalised re-entrant jet length (l_{rj}/h) on Fr_h for ventilated flow.

stream velocity. The high-frequency power law like decay is not affected by change in Re_h, which is consistent with the reasoning that the cavity shedding is controlled by the overlying turbulent boundary layer. If the amount of energy contained within the low- and high-frequency peaks is compared across the range of Re_h, it is observable that peaks have approximately equal value at higher Re_h, but the low-frequency oscillation become increasingly more dominant with decreasing Re_h.

The location of the low-frequency peak does not collapse with St_h. As previously noted, the low frequency peak is associated with the large-scale re-entrant jet oscillation and it may be useful to alternatively define a re-entrant jet length based Strouhal number, $St_{rj} = f l_{rj}/U_\infty$. A plot showing the dependence of re-entrant jet length, non-dimensionalised by fence height (l_{rj}/h), on Fr_h is given for ventilated flow in figure 6. The maximum and minimum recorded length are represented with error-bars for each investigated condition. A linear dependence of l_{rj}/h on Fr_h is evident. The justification for designation of Fr_h as a dimensionless parameter governing the re-entrant jet length can be found if the studied flow is considered as analogous to the recirculating flow associated with the undular jump phenomenon in super-critical open-channel flow. As presented in experimental work by Hager et al. [9], the length of recirculating zone (termed 'roller length') has a dependence on a fixed length scale based Fr which can be closely approximated with a linear fit function.

When the pressure spectra is plotted against the St_{rj} (figure 5b) it can be seen that the low frequency peak collapses to a constant St_{rj} value of about 0.1. The collapse of low-frequency peak to a nominally constant St_{rj} in two-phase flow is in contrast to the observations from single-phase flow, where the 'flapping' oscillation frequency occurs at a constant St_h. This difference can be attributed to the variation in re-entrant jet length (i.e. recirculating zone length) in the two-phase flow, in comparison to a nominally constant length of recirculating zone observed in single-phase flow for $Re_h > 8.5 \times 10^3$ [8]. On this basis, it may be concluded that the influence of gravity, arising from the presence of two phases with substantially different densities, in the recirculating region modulates its dynamic behaviour.

*Corresponding Author, Luka Barbaca: Luka.Barbaca@utas.edu.au

Conclusion

The topology and unsteady behaviour of ventilated and natural cavity flows over a fixed height 2-D wall-mounted fence were investigated for fixed length cavities using still imaging, X-ray densitometry and dynamic surface pressure measurements in two experimental facilities. Based on the observations of cavity topology and shedding mechanisms, the examined flow is classified within the 'thin non-auto-oscillating cavity' regime [5]. Two main features contributing to cavity unsteady behaviour were found, irregular small-scale shedding of gaseous/vaporous structures at the cavity closure and larger-scale oscillations in size of the re-entrant jet affected region. From the spectral analysis of wall pressure fluctuations, the small-scale shedding is associated with a high-frequency broad-band peak and a power law decay ($\propto St^{-7/3}$), analogous to that observed in a single-phase flow over a forward-facing step. The location of this peak collapsed for $St_h \approx 0.02$, showing that the cavity break-up is invariant of Re_h and Fr_h, and governed by the overlying turbulent boundary layer characteristics only. The re-entrant jet oscillation was observed as a low-frequency peak in wall pressure spectra, analogous to the 'flapping' instability of the recirculation zone in single-phase flow. The low-frequency peak was found to collapse for a Strouhal number based on the re-entrant jet length (of about 0.1). The re-entrant length jet was found to have a linear dependence on free-stream velocity, analogous to the recirculation zone length in gravity dominated super-critical open-channel flow. This similarity indicates that the low-frequency oscillation of the re-entrant jet is influenced by gravity (i.e. influence of buoyancy due to inclusion of the gaseous/vaporous phase of much lower density), which is in contrast with the observations from single-phase flow where it was found to be independent of free-stream velocity.

Acknowledgements

The authors wish to acknowledge the assistance of Mr Robert Wrigley and Mr Steven Kent in carrying out the experiments in Univeristy of Tasmania cavitation tunnel, and Mr Kent Pruss and Miss Juliana Wu in carrying out the experiments in University of Michigan cavitation tunnel. The authors wish to acknowledge the financial support received through University of Tasmania Conference and Research Travel Funding Scheme for travel to University of Michigan and the support of Australian Maritime College.

References

[1] Barbaca, L., Pearce, B. W., and Brandner, P. A. (2017a). *Experimental study of ventilated cavity flow over a 3-D wall-mounted fence*. International Journal of Multiphase Flow, 97:10–22.

[2] Barbaca, L., Pearce, B. W., and Brandner, P. A. (2017b). *Numerical analysis of ventilated cavity flow over a 2-D wall mounted fence*. Ocean Engineering, 141:143–153.

[3] Barbaca, L., Pearce, B. W., and Brandner, P. A. (2018). *An experimental study of cavity flow over a 2-D wall-mounted fence in a variable boundary layer* (under revision). International Journal of Multiphase Flow.

[4] Belle, A., Brandner, P. A., Pearce, B. W., de Graaf, K. L., and Clarke, D. B. (2016). *Artificial thickening and thinning of cavitation tunnel boundary layers*. Experimental Thermal and Fluid Science, 78:75–89.

[5] Callenaere, M., Franc, J. P., Michel, J. M., and Riondet, M. (2001). *The cavitation instability induced by the development of a re-entrant jet*. Journal of Fluid Mechanics, 444:223–256.

[6] Franc, J. and Michel, J. M. (2004). *Fundamentals of Cavitation*, volume 76 of Fluid Mechanics and Its Applications. Kluwer Academic Publishers, Dordrecht.

[7] Ganesh, H., Mäkiharju, S. A., and Ceccio, S. L. (2016). *Bubbly shock propagation as a mechanism for sheet-to-cloud transition of partial cavities*. Journal of Fluid Mechanics, 802:37–78.

[8] Graziani, A., Lippert, M., Uystepruyst, D., and Keirsbulck, L. (2017). *Scaling and flow dependencies over forward-facing steps*. International Journal of Heat and Fluid Flow, 67(Part A):220–229.

[9] Hager, W. H., Bremen, R., and Kawagoshi, N. (1990). *Classical hydraulic jump: length of roller*. Journal of Hydraulic Research, 28(5):591–608.

[10] Mäkiharju, S. A., Gabillet, C., Paik, B. G., Chang, N. A., Perlin, M., and Ceccio, S. L. (2013). *Time-resolved two-dimensional X-ray densitometry of a two-phase flow downstream of a ventilated cavity*. Experiments in Fluids, 54(7).

[11] May, A. (1975). *Water Entry and the Cavity-Running Behaviour of Missiles*. Report 75-2, NAVSEA Hydroballistics Advisory Comitee.

[12] Pearce, B. and Brandner, P. (2014). *Inviscid cavity flow over a wall-mounted fence*. Ocean Engineering, 80:13–24.

*Corresponding Author, Luka Barbaca: Luka.Barbaca@utas.edu.au